International Symposium
On Turbulence and Shear Flow
Phenomena (TSFP-9)
June 30 - July 3, 2015 *Melbourne, Australia*

LARGE SCALE ORGANIZATION OF A NEAR WALL TURBULENT BOUNDARY LAYER

Raoul Dekou, Jean-Marc Foucaut, Michel Stanislas
Laboratoire de Mécanique de Lille, Ecole Centrale de Lille
Boulevard Paul Langevin 59655 Villeneuve d'ascq Cédex (France)
raoulflorent.dekoutiomajou@ec-lille.fr

ABSTRACT

An experimental database at a Reynolds number based on momentum thickness Re_θ close to 9800, was obtained in the Laboratoire de Mécanique de Lille wind tunnel with stereo-PIV (SPIV) and hot wire anemometry (HWA) (see Delville *et al.* (2011)); with a Linear Stochastic Estimation procedure based on correlations computation, a 3 component field is reconstructed at high frequency from stereo-PIV at 4Hz and hot wire data at 30kHz. This paper describes the post-processing results of large scale coherent structures (uniform momentum regions and vortices) extracted from the reconstructed PIV field. The structures are characterized (size, intensity and life time), and the results are discussed with emphasis on the spatio-temporal organization of the coherent structures and their energetic contribution to the flow.

INTRODUCTION

Recent numerical studies and experiments have revealed the existence of very long meandering structures consisting of alternance of low and high speed fluid within the logarithmic and wake regions (Abe *et al.* (2004), Ganapathisubramani *et al.* (2006*a*) Hutchins & Marusic (2007*a*) and Lee & Sung (2011)). The terms Large Scale Motion (LSM) and Very Large Scale Motion (VLSM) refer respectively to structures with a streamwise extent of $2-3\delta$ and greater than 3δ. Because they play an important role in the turbulence production across the boundary layer (Ganapathisubramani *et al.* (2003), Ganapathisubramani *et al.* (2005*a*) and Ganapathisubramani *et al.* (2006*b*)) and are thought to be responsible for small scales amplitude modulation near the wall (Hutchins & Marusic (2007*b*)) many authors have investigated them in turbulent wall layers for various flow configurations (zero pressure gradient turbulent boundary layer Hutchins *et al.* (2011) and Hambleton *et al.* (2006), pipe flows Ganapathisubramani *et al.* (2006*a*), channel flows Monty *et al.* (2009)). General conclusions can be drawn from these studies. Firstly, both low and high speed streaks share similarities in averaged size, Sillero *et al.* (2014) have suggested that this is true only for pipe and turbulent boundary layer flows whereas there is a discrepancy among the two structures in channel flows. Conversely, Dennis & Nickels (2011*b*) found that low speed streaks within a zero pressure turbulent boundary layer are slightly longer than high speed ones and their energetic contribution to the Reynolds shear stress $\overline{u'v'}$ is more significiant. Secondly, the structures streamwise length scales on δ, increases with the wall normal distance in the log region and decreases beyond (Ganapathisubramani *et al.* (2003) and Ganapathisubramani *et al.* (2006*a*)). Their spanwise width increases monotonically with the wall normal distance (Lee & Sung (2011)). Together with a detailed analysis of large scale vortices, a large scale motion model was provided in Adrian *et al.* (2000). This model suggests that hairpin-type vortices are bounding regions of low speed fluid with ejections between their legs and sweeps outside (Ganapathisubramani *et al.* (2003), Ganapathisubramani *et al.* (2005*b*), Ganapathisubramani *et al.* (2006*b*)). The hairpins are mostly inclined at $35-40^\circ$ with the streamwise direction (Dennis & Nickels (2011*a*) at 45° as suggested in Ganapathisubramani *et al.* (2005*b*), and Ganapathisubramani *et al.* (2006*b*). On averaged, they are aligned along the streamwise direction to form hairpin packets which move downstream with the same convection velocity. The packets increase in spanwise scale as they evolve downstream. The energetic contribution of the hairpins packets at $Re_\tau = 1060$ was investigated by Ganapathisubramani *et al.* (2003). Packets of hairpins within the logarithmic region were found to contribute to more than 25% of the total stress $-\overline{u'v'}$ even though they occupy less than 4% of the total area. In addition, Lee & Sung (2011) found that the VLSMs contribute approximetaly to 45% of the total Reynolds shear stress included in all patches. It is now obvious that very large scale motions play a crucial role in the turbulence production, however, their characterization is not complete. The spatial resolution of the data and the interrogation window size in PIV set the range of scale that can be resolved. The first parameter defines the size of the smallest eddies detected and the last one sets the maximum size of the eddies, optimizing both of them is difficult and many studies focus on a particular range of scale (Herpin *et al.* (2013) and Gao *et al.* (2011) looked particularly at the small scales). Switching from low and moderate Reynolds numbers to higher ones, the structures size increases. Studies at Reynolds $Re_\tau \approx 1100$ revealed that their streamwise extent is 2δ (Ganapathisubramani *et al.* (2003) and Hambleton *et al.* (2006)), futher studies at Mach 2 (Ganapathisubramani *et al.* (2006*a*)) and $Re_\tau = 6.6\times10^5$ (Hambleton *et al.* (2006)) revealed structures which length can go up to 8δ and 20δ respectively. These long streamwise extents, combined with the three dimensional aspect of the structures and their meandering behaviour complexify their extraction and analysis. Thus, new simulations and PIV experiments with enough spatial resolution and with a large field of view need to be performed at high Reynolds number to complete the existing model. It is for this purpose that an experimental database at high Reynolds number ($Re_\tau = 3610$) was built

Table 1: Main flow properties with δ the boundary layer thickness, u_τ the friction velocity and θ the momentum thickness. The Reynolds numbers are $Re_\delta = \frac{U_\infty.\delta}{\nu}$, $Re_\tau = \frac{U_\tau.\delta}{\nu}$ and $Re_\theta = \frac{U_\infty.\theta}{\nu}$.

Facility	U_∞(m/s)	T(K)	δ(m)	u_τ(m/s)	Re_δ
LML	5.	288	0.28	0.188	96020

Facility	Re_θ	Re_τ
LML	9830	3610

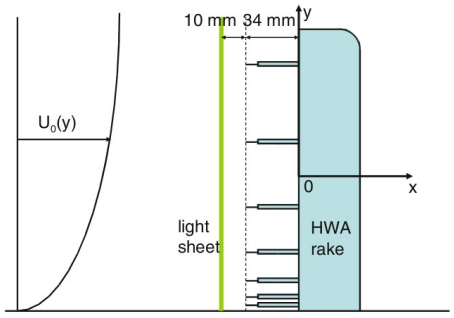

Figure 1: Position of the rake relative to the SPIV measurement plane, probes on the rake are logarithmically distributed in wall-normal direction.

in the frame of the WALLTURB project. Measurements were made in a zero pressure gradient turbulent boundary layer over a flat plate using Stereo PIV at $4Hz$ and Hot Wires Anemometry at $30kHz$. An interesting approach is to use LSE applied to such data in order to reconstruct a fully time-resolved field with 3 velocity components. The first part of the present paper describes briefly the experimental set-up, then the LSE procedure used for reconstruction is described and a statistical validation is performed on the reconstructed field. The last part is dedicated to the characterization of large scale structures extracted from the reconstructed field: a statistical analysis of relevant quantities (diameter, life time, intensity, and Reynolds stress) is carried out on coherent structures and conclusions provided.

EXPERIMENTAL SET-UP

The experiment was carried out in the LML wind tunnel during a WALLTURB test campaign. A full description of this wind tunned can be found in Carlier & Stanislas (2005) and the WALLTURB program is described in Stanislas *et al.* (2012).

The present experiment was carried out with a free stream velocity $U_\infty = 5\ m/s$ and a Reynolds number based on momentum thickness $Re_\theta = 9830$. A Clauser chart fit was used to estimate the friction velocity $u_\tau = 0.188$ corresponding to a Reynolds number based on friction velocity $Re_\tau = 3610$. The hot wire rake (HWR) was positioned streamwise at $x = 18\ m$ from the boundary layer starting point. This hot wire rake is made of 143 single hot wire probes grouped in 13 vertical combs along the spanwise direction z with 11 probes on each of them. The probes are

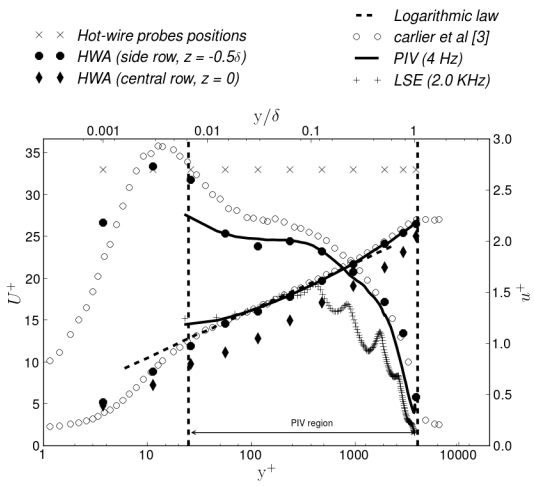

Figure 2: Mean & RMS velocity profiles obtained here compared with those obtained by Carlier & Stanislas (2005) using single hot-wires probes ($l^+ = 11$). The vertical dashed lines indicate the region of the boundary layer in wall-normal direction covered in the present paper, the ($\times$) denote the location of hot-wire probes along a given comb.

logarithmically distributed as shown in Figure 1. The first two rows are below the PIV measurement plane and were not used in the present study. The sensing wires are 0.5 *mm* long and 2.5 μm in diameter ($l^+ = 11.8$ and $d^+ = 0.006$ respectively). The acquisition time of the hot wire signal is 6s, the sampling frequency is 30 KHz and measurements are repeated over 534 blocks to ensure convergence.

Because hot wire measurements are limited to one component, a stereo-PIV system described in Delville *et al.* (2011) allows measurements at 4 Hz, the resulting velocity field has 3 components with a spatial resolution of 2 *mm* in spanwise and wall normal directions. The laser sheet is parallel to the hot wire rake and positioned 1 *cm* upstream of it as shown in Figure 1, it covers the entire log region over an area of $30 \times 30\ cm^2$.

LINEAR STOCHASTIC ESTIMATION

From the hot wire and PIV measurements, the LSE (see e.g. Guezennec (1989)) is used to reconstruct a fully time-resolved 3 component velocity field with the same spatial resolution as the PIV. Given a set of observables located in space at x' and in time at t', the LSE allows the linear approximation of the conditional estimate of some quantity at a position x and time t. In our case, the conditional variables to reconstruct at high frequency are the three components of the velocity $\mathbf{u}'(t,\mathbf{x}) = (u'_1,u'_2,u'_3)(t,\mathbf{x})$ in the PIV y-z plane. The set of observables includes the streamwise velocity $u'_1(t',\mathbf{x}')$ measured at the N_h hot-wires probes on the two dimensional rake whose coordinates are given by $\mathbf{x}' = (x'_1,...,x'_{N_h})$. A multitime formulation for the linear approximation of the velocity component $\hat{u}_i(t,\mathbf{x})$ is implemented, such as used in Durgesh & Naughton (2010):

$$\hat{u}_i(t',\mathbf{x}) = \sum_{k=1}^{N_h} u'_1(t'+\tau(x'_k),x'_k).a_{k,i}(\mathbf{x}) \qquad i = 1,2,3 \tag{1}$$

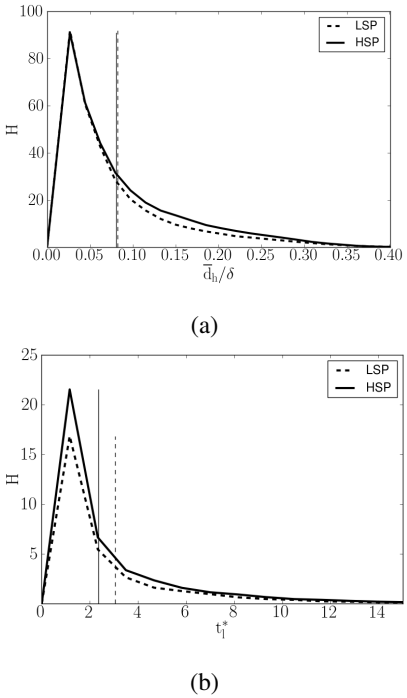

Figure 3: Low and high momentum regions a) mean hydraulic diameter histogram and (b) life time histogram.

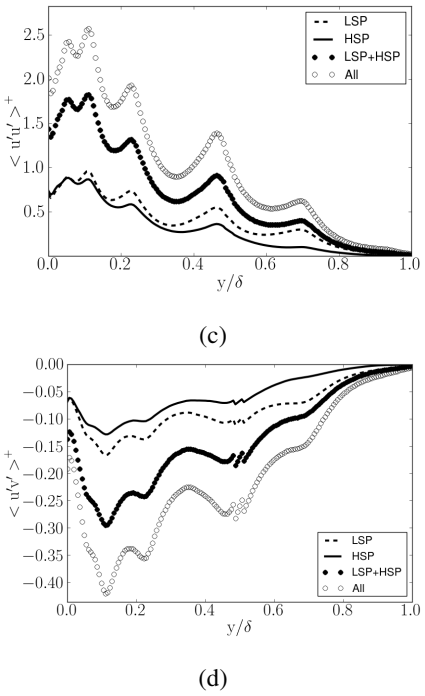

Figure 4: Low and high momentum regions (a) streamwise Reynolds stress contribution compared with the total stress and (b) Reynolds shear stress contribution compared with the total stress.

Where $a_{k,i}(\mathbf{x})$ are coefficients relating the conditional field to the observers, and $\tau(\mathbf{x}')$ is the time delay which maximises the streamwise correlation between a point x in the PIV plane and an observer x'. A Ridge regression is used to solve the linear equation defined by equation (1) in order to find the best $a_{k,i}(\mathbf{x})$ coefficients to estimate the space-time resolved velocity field $\hat{u}_i(t',\mathbf{x})$. Note that the same time delay was used here for the streamwise, spanwise and wall normal velocity components.

STATISTICAL ANALYSIS OF THE VELOCITY FIELD

In order to characterize the quality of the reconstructed data, a statistical analysis was performed on the PIV, HWR and reconstructed data and compared to those of Carlier & Stanislas (2005).

In a previous analysis of the present PIV and HWR data, Tutkun *et al.* (2009) did show that the HWR generates an obstruction which is maximum in the plane of symmetry and affects mostly the mean velocity field. For this reason, the side rows of the HWR are used here for comparison to minimize the influence of the obstruction. Figure 2 displays profiles of mean U^+ and root mean square (RMS) u^+ velocities. For the mean velocity, a good match is observed with Carlier & Stanislas (2005) and the logarithmic law with $\kappa = 0.41$ and $C = 4.9$. The central row is also plotted to illustrate the blockage effect. Concerning the RMS, a good match is observed between all rows of the HWR and the PIV data. A slight underestimation is visible compared to Carlier & Stanislas (2005). The RMS reconstructed by LSE at 2.0 KHz displays an underestimation and wavy patterns. Each crest corresponds to a hot wire probe position highlighted by the crosses on the top part of the figure. Because the LSE is based on spatio-temporal correlations between the hot wire signal and the original PIV field, points in the PIV domain which are between two hot wire probes are less correlated and thus lead to lower amplitudes. The R.M.S of the reconstructed field follows the same trend as the one obtained by Carlier & Stanislas (2005) but its amplitude is lower denoting a loss of energy. Part of it is also due to the filtering of the small scales by LSE reconstruction. Also the PIV plane and the HWA are separated streamwise by $\Delta x = 1$ cm ($\Delta x^+ = 129$), therefore the correlation between the PIV and hot wire measurements reaches values close to 0.8 and not 1 as might be expected.

The following paragraphs describe only statistical results obtained on large scale coherent structures extracted from the reconstructed field. For details regarding the extraction algorithms, the reader is referred to (Dekou (2015)) .

CHARACTERIZATION OF LOW AND HIGH MOMENTUM REGIONS

Figures 3 (a) and (b) respectively display the histogram of the mean hydraulic diameter $\overline{d}_h/\delta$ of low and high momentum regions (dashed and plain lines respectively) normalized with the boundary layer thickness δ and the histogram of their life time t_l^* normalised with the external velocity and the boundary layer thickness. From figure 3 (a), it is obvious that the mean hydraulic diameter of low and high momentum regions follow the same trend with a common peak at $\bar{d}_h = 0.026\delta$ and a mean value of $\bar{d}_h = 0.081\delta$ (vertical lines). In Figure 3 (b), the life time histogram are similar but the one from low momentum region is slightly

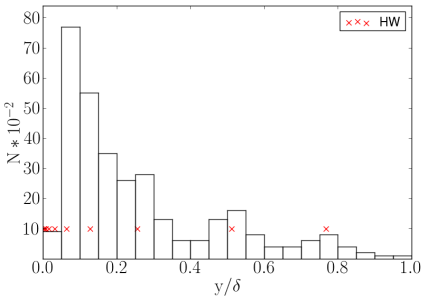

Figure 5: Number of vortex detected against the wall normal position.

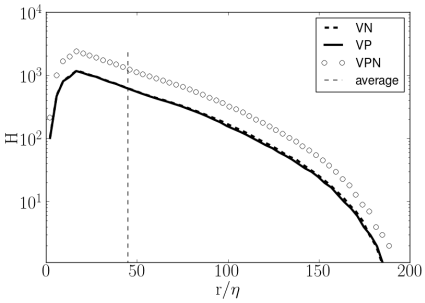

Figure 6: Histogram of the vortex radius scaled in Kolmogorov units with the mean radius plotted in vertical dashed line. (VP) Positive vortex , (VN) negative vortex and (VPN) both positive and negative vortex.

shifted toward longer times with a shorter peak. This difference may either be a result of lack of convergence or reflects the true physics within the flow. As it was mentionned in the introduction, studies in the literature do not agree on this point. Dennis & Nickels (2011*b*) found that low speed streaks were slightly shorter than high speed ones and argued that the hairpins heads strengthen the length of low speed streaks. Although the scale range is different from the one in the present study, the observations match well. More experiments or DNS need to be perfomed to confirm this.

Figures 4 (a) and (b) display the streamwise and shear Reynolds stresses contribution from low and high momentum regions (dashed and plain lines respectively) separately, compared to the total stresses (empty circles). The joined contribution is also plotted (filled circle). The contributions from both regions are comparable for both types of stresses. Globally, the contribution from low and high momentum regions to $< u^{'}u^{'} >$ is of order of 42% and 24% respectively, which means that a large part of this Reynolds stress is generated inside these two types of structures. Remarkably, the high momentum regions contribution decreases almost linearly with wall distance while the low momentum regions one is nearly constant. For $< u^{'}v^{'} >$, the contribution from low momentum regions is 43% and the one from high momentum ones is (23%). Again, the two contributions are comparable close to the wall and the high momentum regions one decreases rapidly with wall distance. The fact that the energetic contribution from low speed streaks is more important than the one from high speed ones is not new and was reported in Dennis & Nickels (2011*b*) for the shear stress only. Also, the 23% contribution to the shear

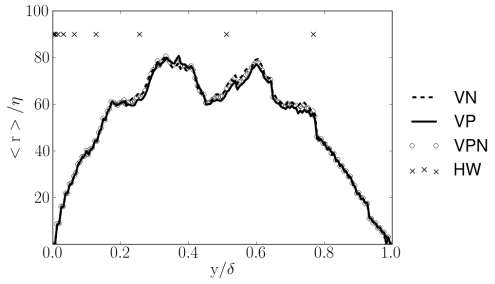

Figure 7: Wall normal evolution of the mean radius scaled in Kolmogorov units, the hot wire probes positions are plotted with crosses. (VP) Positive vortex , (VN) negative vortex and (VPN) both positive and negative vortex.

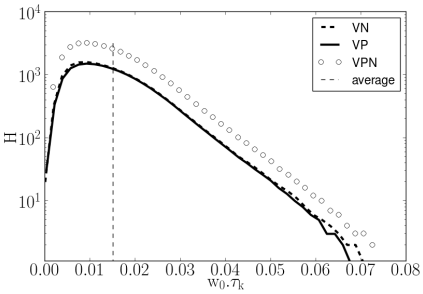

Figure 8: Histogram of the vortex vorticity scaled in Kolmogorov units with the mean vorticity plotted in vertical dashed line. (VP) Positive vortex , (VN) negative vortex and (VPN) both positive and negative vortex.

stress obtained here is close to the 25% obtained by Ganapathisubramani *et al.* (2003) at $Re_\tau = 1060$ even though the scale range is different.

CHARACTERIZATION OF VORTICES

Figure 5 displays the number of vortices against the wall normal position sampled in 20 intervals. As it was shown that there is a loss of energy between hot wire probes positions, these are displayed with red crosses to see if they affect the number of vortices detected. For the first sample close to the wall, despite a high concentration of probes in the region, the number of vortices is low compared to the other regions, this can be justified by the fact that the the PIV field starts at 4*mm* from the wall. Small vortices whose centers are located on the border (or very closed to it) could not be processed and are not taken into account in the distribution. A peak is observed for y/δ in $[0.05, 0.1]$ and globally the number of vortices detected decreases away from the wall. We can also observe that close to the probes, for example at y/δ in $[0.45, 0.55]$ and $[0.7, 0.8]$ the vortices detected are more numerous than between the probes for example at y/δ in $[0.35, 0.45]$ and y/δ in $[0.6, 0.7]$ where a loss of energy was noted due to LSE filtering. Thus, in these regions the number of vortices detected should be readjusted towards higher values and the evolution would provide a smoother decreasing trend with the wall distance. Figure 6 displays

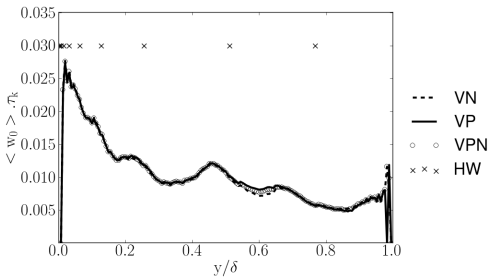

Figure 9: Wall normal evolution of the mean vorticity scaled in Kolmogorov units, the hot wire probes positions are plotted with crosses. (VP) Positive vortex , (VN) negative vortex and (VPN) both positive and negative vortex.

the histogram of the radius scaled in Kolmogorov units. Globally, small vortices are more numerous than large ones but at very small radius (below 16.62η) this tendency is reversed, a mean value is found at 45η. This value is far above that of $7-12\eta$ and $5-6\eta$ reported in Herpin *et al.* (2013) and in Gao *et al.* (2011) respectively. It suggests that larger vortices exist within the turbulent boundary layer. Figure 7 displays the evolution of the mean radius of vortices scaled in Kolmogorov units with wall distance. The hot wire probes positions are also displayed. The two peaks observed at $y \approx 0.33\delta$ and at $y \approx 0.6\delta$ are located in between the hot wire probes, inside regions where the number of vortices detected is low compared to the others, notably the ones with small sizes. This probably comes from the LSE filtering in between the probes and it suggests that the values at the two peaks should have lower amplitude. The deep observed at $y \approx 0.45\delta$ is close to a probe position in a region where the velocity field is less filtered and the number of vortices detected is important. Thus the radius of 60η obtained at this position is more likely to be representative of the real flow. Above $y \approx 0.8\delta$ the number of vortices detected is low compared to the other regions. The mean radius obtained in this range should be taken with caution.

Figure 8 displays the histogram of the vorticity scaled in Kolmogorov units. This histogram presents a log-normal behaviour like the ones reported in Herpin *et al.* (2013) for smaller vortices. A peak is found at $0.009/\tau_k$ with a mean vorticity of $0.015/\tau_k$ which is far below the value of $1.5/\tau_k$ obtained in Herpin *et al.* (2013). Figure 9 displays the evolution of the mean vorticity scaled in Kolmogorov units against the wall normal position. As for the radius there is an evident correlation between the oscillation observed on this curve and the hot wire probes positions. The deeps observed in Figure 9 are located in between the hot wire probes inside regions where the number of vortices detected is lower, especially the ones with low vorticity. As mentioned before, these regions are subjected to a LSE filtering, and, therefore, the amplitude of the mean vorticity is underestimated. The peaks of the mean vorticity are located close to the hot wire probes positions where the number of vortices detected is important, thus, the values obtained are more likely to be representative of the real flow. Above 0.8δ the number of vortices detected is lower and the values obtained for the mean vorticity should be taken with caution.

CONCLUSION

Time resolved hot wire rake measurements at 30 KHz were combined with SPIV measurements at 4 Hz to reconstruct via LSE a 3 component velocity field resolved in space and time. A statistical analysis perfomed on the outcoming field shows that LSE leads to a loss of energy affecting most scales but keeping the large scales of interest. Coherent structures extraction reveals that low and high momentum regions are bordered by counter-rotating vortex pairs. Low momentum regions are found to be slightly more energetic and longer than the high momentum ones but on average, their cross sections are nearly equal. It is also found that the contribution of streaks to the Reynolds stresses are important, about 42% for low speed and 23% for high speed. The vortices detected have larger sizes and a smaller vorticity than the ones commonly reported in the literature typically 45η and $0.015/\tau_k$. The perspective of this study is to complete the modelization of these large scale coherent structures. Similar analysis will be performed at a Reynolds of $Re_\theta = 20000$ and for a bump turbulent boundary layer to see respectively the Reynolds and and pressure gradient effect on the structures. Besides, for each flow configuration their origin and interaction with the small scale structures near the wall will be carefully examined.

REFERENCES

Abe, Hiroyuki, Choi, Haecheon & Kawamura, Hiroshi 2004 Very large-scale structures and their effects on the wall shear-stress fluctuations in a turbulent channel flow up to reτ= 640. *Journal of Fluids Engineering* **126** (5), 835–843.

Adrian, RJ, Meinhart, CD & Tomkins, CD 2000 Vortex organization in the outer region of the turbulent boundary layer. *Journal of Fluid Mechanics* **422**, 1–54.

Carlier, Johan & Stanislas, Michel 2005 Experimental study of eddy structures in a turbulent boundary layer using particle image velocimetry. *Journal of Fluid Mechanics* **535**, 143–188.

Dekou, Raoul 2015 Large scale organization of a near wall turbulent boundary layer. PhD thesis, Ecole Centrale de Lille.

Delville, Joel, Braud, Patrick, Coudert, Sebastien, Foucaut, Jean-Marc, Fourment, Carine, George, WK, Johansson, Peter BV, Kostas, Jim, Mehdi, Fahrid, Royer, A *et al.* 2011 The wallturb joined experiment to assess the large scale structures in a high reynolds number turbulent boundary layer. In *Progress in Wall Turbulence: Understanding and Modeling*, pp. 65–73. Springer.

Dennis, David JC & Nickels, Timothy B 2011*a* Experimental measurement of large-scale three-dimensional structures in a turbulent boundary layer. part 1. vortex packets. *Journal of Fluid Mechanics* **673**, 180–217.

Dennis, David JC & Nickels, Timothy B 2011*b* Experimental measurement of large-scale three-dimensional structures in a turbulent boundary layer. part 2. long structures. *Journal of Fluid Mechanics* **673**, 218–244.

Durgesh, V & Naughton, JW 2010 Multi-time-delay lsepod complementary approach applied to unsteady high-reynolds-number near wake flow. *Experiments in fluids* **49** (3), 571–583.

Ganapathisubramani, B, Clemens, NT & Dolling, DS 2006*a* Large-scale motions in a supersonic turbulent boundary layer. *Journal of Fluid Mechanics* **556**, 271–282.

Ganapathisubramani, B, Hutchins, N, Hambleton, WT, Longmire, EK & Marusic, I 2005*a* Investigation of large-scale coherence in a turbulent boundary layer using two-point correlations. *Journal of Fluid Mechanics* **524**, 57–80.

Ganapathisubramani, Bharathram, Longmire, Ellen K & Marusic, Ivan 2003 Characteristics of vortex packets in turbulent boundary layers. *Journal of Fluid Mechanics* **478**, 35–46.

Ganapathisubramani, Bharathram, Longmire, Ellen K & Marusic, Ivan 2006*b* Experimental investigation of vortex properties in a turbulent boundary layer. *Physics of Fluids (1994-present)* **18** (5), 055105.

Ganapathisubramani, Bharathram, Longmire, Ellen K, Marusic, Ivan & Pothos, Stamatios 2005*b* Dual-plane piv technique to determine the complete velocity gradient tensor in a turbulent boundary layer. *Experiments in Fluids* **39** (2), 222–231.

Gao, Q, Ortiz-Duenas, C & Longmire, EK 2011 Analysis of vortex populations in turbulent wall-bounded flows. *Journal of Fluid Mechanics* **678**, 87–123.

Guezennec, YG 1989 Stochastic estimation of coherent structures in turbulent boundary layers. *Physics of Fluids A: Fluid Dynamics (1989-1993)* **1** (6), 1054–1060.

Hambleton, WT, Hutchins, N & Marusic, Ivan 2006 Simultaneous orthogonal-plane particle image velocimetry measurements in a turbulent boundary layer. *Journal of Fluid Mechanics* **560**, 53–64.

Hansen, Per Christian 1994 Regularization tools: A matlab package for analysis and solution of discrete ill-posed problems. *Numerical algorithms* **6** (1), 1–35.

Herpin, Sophie, Stanislas, Michel, Foucaut, Jean Marc & Coudert, Sebastien 2013 Influence of the reynolds number on the vortical structures in the logarithmic region of turbulent boundary layers. *Journal of Fluid Mechanics* **716**, 5–50.

Hutchins, N & Marusic, Ivan 2007*a* Evidence of very long meandering features in the logarithmic region of turbulent boundary layers. *Journal of Fluid Mechanics* **579**, 1–28.

Hutchins, Nicholas & Marusic, Ivan 2007*b* Large-scale influences in near-wall turbulence. *Philosophical Transactions of the Royal Society A: Mathematical, Physical and Engineering Sciences* **365** (1852), 647–664.

Hutchins, N, Monty, JP, Ganapathisubramani, B, Ng, HCH & Marusic, I 2011 Three-dimensional conditional structure of a high-reynolds-number turbulent boundary layer. *Journal of Fluid Mechanics* **673**, 255–285.

Lee, Jae Hwa & Sung, Hyung Jin 2011 Very-large-scale motions in a turbulent boundary layer. *Journal of Fluid Mechanics* **673**, 80–120.

Monty, JP, Hutchins, N, Ng, HCH, Marusic, I & Chong, MS 2009 A comparison of turbulent pipe, channel and boundary layer flows. *Journal of Fluid Mechanics* **632**, 431–442.

Sillero, Juan A, Jiménez, Javier & Moser, Robert D 2014 Two-point statistics for turbulent boundary layers and channels at reynolds numbers up to $\delta+$ 2000. *Physics of Fluids (1994-present)* **26** (10), 105109.

Stanislas, Michel, Foucaut, Jean-Marc, Coudert, Sebastien, Tutkun, Murat, George, William K & Delville, Joel 2011 Calibration of the wallturb experiment hot wire rake with help of piv. In *Progress in Wall Turbulence: Understanding and Modeling*, pp. 75–84. Springer.

Stanislas, Michel, Jimenez, Javier & Marusic, Ivan 2012 Progress in wall turbulence: Understanding and modeling proceedings of the wallturb international workshop held in lille, france, april 21-23, 2009 .

Tutkun, Murat, George, William K, Foucaut, Jean-Marc, Coudert, Sébastien, Stanislas, Michel & Delville, J 2009 In situ calibration of hot wire probes in turbulent flows. *Experiments in fluids* **46** (4), 617–629.